12

Doppler Wind Lidar

Christian Werner

Institut für Physik der Atmosphäre, DLR Deutsches Zentrum für Luft- und Raumfahrt e.V. Oberpfaffenhofen, D-82234 Wessling, Germany
(christian-werner@gmx.de)

12.1 Introduction

The change of perceived frequency of radiation when the source or the receiver move relative to one another is a well-known phenomenon. First described by Austrian physicist Christian Doppler (1803–1853) for acoustic waves, it occurs for electromagnetic waves as well. If the change of frequency can be measured, the relative speed of the source with respect to the receiver can be determined, provided the group velocity of the radiation in the respective medium is known. As the speed of light in air and vacuum has been known with high accuracy, the optical Doppler effect lends itself ideally to the remote measurement of the speed of very distant or otherwise uncooperative objects. If the object does not move directly toward or directly away from the observer, then the use of the optical Doppler effect clearly yields the component of the speed of the object along the line of sight.

It is obvious that for a velocity measurement the object must emit electromagnetic radiation. This is the case for stars and galaxies; perhaps the most spectacular application of the optical Doppler effect was the determination of the shift of light from distant stars, all toward longer wavelengths, leading to our present notion of an expanding universe. Because the relative shift of optical frequencies, $\Delta f/f$, is proportional to v/c, the ratio of the velocity v of the object to the speed of light c, and because very distant stars move away fast, these measurements were comparatively easy to make.

Velocity determinations on Earth and in the Earth's atmosphere are more difficult for two reasons. First, the objects whose speed is to be

measured must be made to emit radiation. This can be done, e.g., by illumination. Second, the shift of the return radiation with respect to the transmitted radiation must be determined. Velocities of interest on Earth vary greatly with object and purpose. The movement of air masses, e.g., is interesting at velocities of about 0.1 to 100 m/s which, relative to the speed of light of 3×10^8 m/s, amounts to a fraction of roughly 3 parts in 10^{10} to 3 parts in 10^7. This is not easy to measure unless very narrow spectral lines and highly sophisticated equipment are used.

Although optical Doppler measurements have a multitude of terrestrial applications such as the determination of the speed and vibrations of moving parts in traffic, in industrial production, in machine shops, etc., this chapter is exclusively devoted to the measurement of the movement of atmospheric air masses, or wind and turbulence, from the observation of aerosols. Compared with other Doppler measurements, Doppler wind measurements have the additional problems that the illumination of the air even with powerful sources yields very weak return signals and that the return signals must be analyzed not just for wavelength, but for distance as well. Following this Introduction, Section 12.2 will briefly recall the notations and formulas that will be used in connection with optical Doppler wind lidar. In Section 12.3 different schemes for remote measurements of the wind vector are presented. In Section 12.4 the wavelengths to be used, the different detection schemes and the various scan techniques for Doppler lidar are discussed. Section 12.5 shows several applications, with main emphasis on heterodyne wind lidar, and Section 12.6 concludes this chapter with a number of new areas in which optical Doppler wind lidar may gain importance in the future.

12.2 The Optical Doppler Effect

Light, unlike sound, is not "advected" by some medium. In the optical Doppler effect, there is therefore no distinction between the case of the moving transmitter and the moving receiver, or both transmitter and receiver moving in a medium. If the emitted light has wavelength λ_0 and frequency $f_0 = c/\lambda_0$ and the relative speed along the line of sight is v, then the observed frequency is

$$f = f_0(1 + v/c). \tag{12.1}$$

Air and aerosols, however, normally do not emit light, but for a measurement of their speed are illuminated by light from the lidar transmitter.

If that light has frequency f_0, then its apparent frequency on the aerosol particle is given by Eq. (12.1). Clearly, the light is reemitted, or backscattered, at this frequency, which then, because the particle is moving while scattering, is detected by the lidar receiver as being shifted to frequency

$$f = f_0 + \Delta f = f_0(1 + 2v/c). \tag{12.2}$$

We define the particle (or wind) velocity in such a way that a movement *toward* the lidar which leads to a *positive* frequency shift is characterized by a *positive* line-of-sight velocity, and vice versa. Instead of the line-of-sight velocity v_{LOS} or velocity component along the line of sight, we occasionally use the term "radial velocity" v_{r} or radial component of a velocity vector that is not parallel to the line of sight. v_{LOS} and v_{r} are fully synonymous, with the same sign convention.

Now the collective movement of air masses which we call wind is superimposed by the individual, thermal, random movement of the molecules. These normally move must faster than the wind speed and so much the faster the higher the temperature. The relative shift of their velocity distribution with the wind speed is therefore small. Aerosol particles, because of their higher mass, move more slowly at the same temperature and have therefore a narrower velocity distribution. They are shifted by the same amount, but relative to its width this shift is much larger and amenable to measurement. The situation is schematically shown in Fig. 12.1.

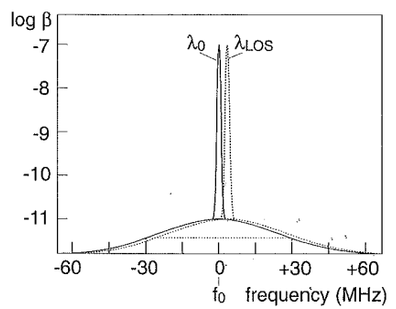

Fig. 12.1. Schematic representation of the original (solid) and wind-shifted (dotted) frequency distributions. If there are aerosols present, a narrow spike is superimposed onto the broad molecular peak. The return-signal frequency is shifted here toward higher values, indicating that the wind comes toward the lidar. At 10.59 μm wavelength, the 3-MHz shift corresponds to roughly 20 m/s.

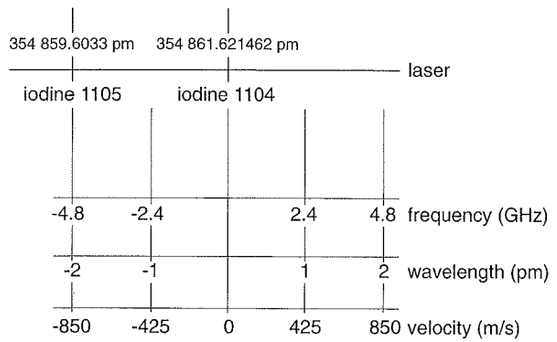

Fig. 12.2. Relation of wavelength, frequency and wavelength shift with wind speed for Doppler wind lidar measurements with a frequency-doubled Nd:YAG laser stabilized to the iodine 1104 atomic transition. Note that wind speed scale is a factor >1000 too coarse for most practical applications.

To give an idea how small wind-induced shifts are relative to the absolute wavelengths or frequencies and to demonstrate that lidar transmitters and receivers must be controlled to sub-picometer accuracy, Fig. 12.2 shows how wind velocities (bottom scale) translate into wavelength shifts and frequency shifts (center scales) if light from a frequency-tripled Nd:YAG laser is used. The top scale shows the positions of two iodine lines (often designated as # 1105 and # 1104) to which the laser can be stabilized [1]. In direct-detection lidars and in the field of optical space communication it is necessary to stabilize the laser with respect to the filters in front of the detectors.

12.3 Brief Overview of Wind Lidar Measurement Schemes

Pulsed Doppler wind lidar is not the only method for the remote optical measurement of wind speed. There are other optical methods that shall be briefly presented here for the sake of completeness. They will not be treated in detail because their application is limited to short range due the very principle of the measurement, because the method is relatively new and its technical implementation is complicated and still in its infancy, or because they are described elsewhere in this book.

12.3.1 Crosswind Determination by Pattern Correlation

Cloud droplets and aerosol particles are not distributed homogeneously in the atmosphere. Smokestack plumes and clouds show patterns easily recognized with the naked eye. If images of such patterns are taken at two points in time, t_1 and t_2, and if the geometric parameters such as distance, angle of observation, and imaging scale are known so that the two-dimensional pattern $H(x, y)$ of the object can be determined from the images, then it is sufficient to find those two values (ξ, η) by which the second image must be shifted to give maximum similarity with the first. Or in mathematical terms, we need to determine those values (ξ, η) that maximize the cross-correlation coefficient of the two images:

$$Q(\xi, \eta) = \iint H(x, y, t_1) H(x - \xi, y - \eta, t_2)\, \mathrm{d}x\, \mathrm{d}y = \text{maximum}. \tag{12.3}$$

The (two-component) velocity vector in the plane perpendicular to the line of sight (normally the horizontal plane) is then given by the simple relation

$$\mathbf{u}_{\text{hor}} = \frac{1}{t_2 - t_1}(\xi, \eta). \tag{12.4}$$

We shall not dwell on the fact that instead of the convolution of Eq. (12.3) fast Fourier transform algorithms are the preferred method to obtain the shift parameters (ξ, η).

The method can be used in the daytime in an entirely passive way, but only for the altitude at which the receiver sees a smokestack plume or cloud patterns. By selecting an appropriate wavelength it is possible to make the method particularly sensitive for one type of object: uv for SO_2, visible for clouds and black smoke, ir for very warm plumes. Outside plumes and for nighttime measurements the objects can be illuminated. More efficient than the use of searchlights have been scans of the scene with pulsed lasers. By using a time-resolving detector, height-resolved, and, that is, genuine lidar measurements are possible with this technique. Using a pulsed ruby laser, in fact, Sroga et al. [2] could measure vertical profiles of the horizontal wind vector between 120 and 600 m height as early as 1980. In those days scanning was not possible fast enough for the scan of a set of pictures to be completed in a time $\ll t_2 - t_1$, but Sasano et al. [3] soon developed a correction algorithm for the resulting error. Today, with much more powerful equipment and much faster

computers available, the technique has been developed to a high degree of sophistication (cf. Chapter 5 of this book).

12.3.2 Laser Time-of-Flight Velocimetry (LTV)

If two laser beams are focused at some distance from the ground and close to each other and an aerosol particle crosses both foci, then two flashes can be seen, the interval between the flashes being indicative of the speed of the particle. Because aerosol particles are advected with the wind, the wind speed can be obtained in this way.

It is not obvious that, for a given wind direction, particles will cross both foci unless their connecting line happens to coincide with the wind direction. If the distance between foci is sufficiently small, however (on the order of 1 mm), then there is sufficient scatter in the direction of the particle trajectories to provide useful results. The depth of the focal volume is in any case much larger than its lateral dimensions, so a vertical component of the particle velocity vector is not critical. By rotating the apparatus 90° or by some other measure [4] the perpendicular component of the wind can be determined in the same way. From both results the wind direction and wind speed can then be inferred. The technique has been tested with argon ion lasers of 500 and 200 mW cw power at wavelengths of 514 and 488 nm; maximum range was 70 and 100 m, respectively [4, 5]. The theory of the method was treated in great detail by She and Kelley [6]. In spite of its simplicity, it has not nearly found the same degree of acceptance as a similar technique, laser Doppler velocimetry (see below).

12.3.3 Laser Doppler Velocimetry (LDV)

For moderate distances the horizontal component of the wind vector can also be determined by a method known as laser Doppler velocimetry (LDV). Its principle is similar to that of LTV in that the speed of aerosol particles is also inferred from the time between successive flashes the particles emit when crossing areas of high and low optical intensity. The difference is that in LDV not just two foci, but a large field of interference fringes is used for illumination. Such fields can be obtained from a laser if its beam is divided in two and the fractions are transmitted by different optics oriented at a small angle with respect to one another. The resulting interference pattern acts as a periodic field of regions with high and low intensity. Particles that cross it manifest themselves by

periodic scattering of light with a frequency that is proportional to their speed.

The technique can also be used in two and three dimensions if the volume of interest is illuminated by light of different color and one color-sensitive detector is used for each dimension. For two dimensions the geometry can be relatively simple, with the axes of the two pairs of beams parallel and the connecting lines between each pair of transmitters perpendicular to one another. If the third dimension is required, the arrangement gets more complicated.

LDV is a method for the measurement of the velocity component *transverse* to the laser beam axis. The mathematical formalism, however, results in formulas that are formally identical with those developed in Section 12.2, hence the expression laser *Doppler* velocimetry. Details of the method are found, e.g., in [7] and [8].

12.3.4 Continuous-Wave Doppler Lidar

Continuous-wave lasers have also been used for the measurement of the longitudinal, or line-of-sight, component of the wind vector using techniques similar to those for genuine pulsed Doppler wind lidar as will be described in the remaining sections of this chapter. In cw Doppler wind lidar depth information is obtained by purely geometric means. If the detection system is focused to distance x, then roughly half of the backscatter signal is generated in a depth range

$$\Delta x = \frac{4x^2\lambda}{A} \tag{12.5}$$

if A is the detector area and λ the wavelength [9]. For a telescope diameter of 500 mm the depth uncertainty at a distance of 100 m is thus only 2 m which is quite good, but 200 m at 1000 m distance which is unacceptable. Although the applicability of the method has been demonstrated not just for ground-based [10], but for airborne systems as well [11–13], its use in practical applications is limited to distances well below 1000 m.

12.3.5 Pulsed Doppler Lidar

The restrictions of methods described in Subsections 12.3.1–12.3.4 are not given for pulsed Doppler lidar. If the term "Doppler lidar" is used in connection with wind measurements, it is implicitly understood that pulsed Doppler lidar is what the speaker has in mind. Pulsed Doppler

lidar has so much greater capabilities for the truly remote measurement of air movements that all other optical techniques of measuring air speed are practically confined to applications in the laboratory, in the machine shop, in production facilities, in wind tunnels, etc., but are hardly ever used in the free atmosphere.

12.4 Doppler Wind Lidar Detection and Scan Techniques

12.4.1 Wavelength Considerations

In Doppler wind lidar the laser wavelength can be chosen at random. However, because the aerosol contribution to the return signal is much better suited for frequency analysis than the molecular signal, the choice of the wavelength to be used will depend on the expected magnitude of the return signal and the expected ratio of aerosol-to-molecular backscatter. The molecular signal is proportional to λ^{-4}, the aerosol signal, depending on wavelength range and particle properties, to something between λ^{-2} and λ^{+1}. Thus, even if the aerosol return decreases with an increase in wavelength, the molecular "background" decreases much faster so the aerosol-to-molecular backscatter ratio gets more favorable.

Figure 12.3 shows simulated spectra (see also Section 6.1) of the return signals obtained with a spaceborne lidar with frequency-tripled (355-nm) Nd:YAG laser for two height bins. A high-resolution system which uses the narrow aerosol peak will work well for medium heights of 2–3 km, but not at high altitudes between 9 and 10 km where fewer aerosol particles are present. Figure 12.3 also shows that despite the shorter distance to the lidar, much fewer photons come back from the higher than from the lower interval because of the decrease of air density with height.

12.4.2 Detection Techniques

Direct Detection

As can be seen from Fig. 12.3, situations may occur in which the molecular part of the backscatter spectrum must be used. This part is frequently referred to as the Rayleigh component (as opposed to the aerosol part, which is often called Mie component) and approximated by a gaussian. The gaussian distribution is a good approximation because thermal motion of the molecules, not the effects of collisions, is the dominating

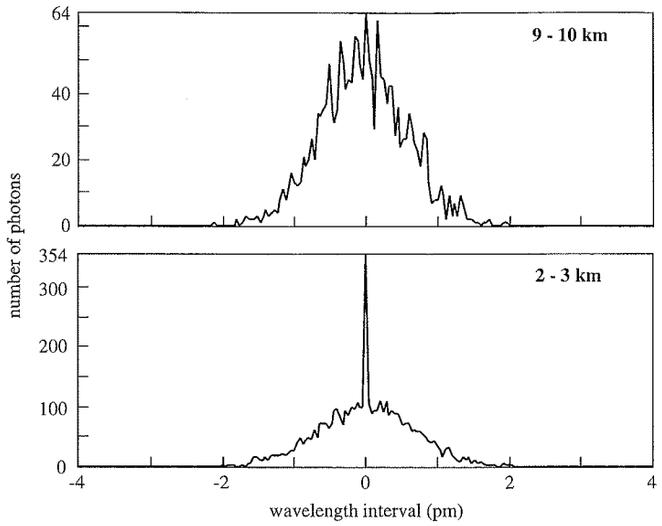

Fig. 12.3. Simulated return spectra for a spaceborne lidar operating at a wavelength of 355 nm. Spectra from 2 to 3 (bottom) and 9 to 10 km height (top) for zero line-of-sight wind speed.

source of line broadening and because collective effects responsible for Brillouin scattering cannot be neglected for accurate wind estimates [14].

For the determination of the center of the distribution from which the wind speed v is obtained by inversion of Eq. (12.2), different techniques are available. One is the use of a high-dispersion multichannel spectrometer that yields the whole distribution which is then submitted to a least-squares gaussian fit. Another is the use of filters such as Fabry–Perot interferometers or etalons [15–18]. Because the shifts are so small these filters must be operated on the edge of the transmission curve where the change of filter transmission with wavelength is maximum. Because the dynamic range of the signals is so large the filters must be as nearly identical as possible, except for the center wavelength of the transmission curves. For high transmitted intensity the transmission curve should cover as much as possible of the respective half of the lidar return signal. To avoid perturbations from the central Mie peak, the transmission function should be zero at line center even under conditions of nonzero wind when the Mie peak shifts from its zero-wind position.

The principle of the technique is depicted in Fig. 12.4. We call the power, or energy, or number of photons counted after transmission through filter 1 and filter 2, A and B. The difference $A - B$, normalized to their sum $A + B$, or

$$q = \frac{A - B}{A + B} = f(v), \tag{12.6}$$

depends in a unique way on wind speed v. Ideally, when this function f is inverted, it could directly yield the line-of-sight speed v. However, the measured values A and B are contaminated by background a and b. Under favorable experimental conditions this background can be measured [15] and subtracted from the apparent values A and B. The situation is more critical if the Mie peak has an intensity not negligible with respect to that of the Rayleigh peak. Let us call its contribution to the apparent values A and B for zero LOS velocity ($v = 0$) a_1 and b_1. When the whole distribution and the Mie peak with it begin to shift to some value $v < 0$ (which corresponds to a frequency shift <0 and a wavelength shift >0 as indicated by the dotted line in Fig. 12.4, a_1 will decrease and b_1 will increase, but not by the same amount. The following parameters must thus be available for use of a direct-detection Doppler wind lidar:

- the difference between laser wavelength and etalon transmission line center wavelengths,
- the background values in channels A and B,

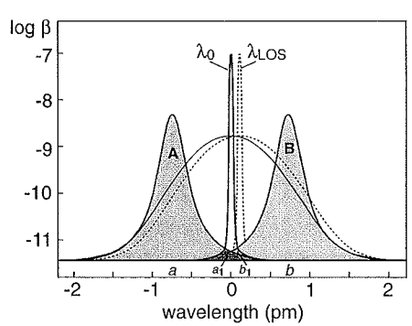

Fig. 12.4. Schematic representation of spectrum components in a direct-detection Doppler wind lidar.

- the temperature, and
- the aerosol scattering ratio.

The latter three parameters change dramatically with altitude, so height profiles are needed. For practical use the background must be known to an accuracy of 1–2%, the temperature which is necessary for the determination of the width of the gaussian to 1 K, and the aerosol scattering ratio, i.e., the ratio of the intensities of the aerosol backscatter to the sum of molecular and aerosol backscatter, to about 5%.

The use of direct-detection Doppler wind lidar thus represents a considerable challenge. And yet a technical implementation of a uv direct-detection lidar has been proposed by Schillinger et al. [19] which is to use the double-edge direct detection technique [17, 20].

The system is schematically depicted in Fig. 12.5. To achieve the required frequency stability, ultrastable radiation from a low-power seed laser is injected into the transmitter laser. Its output pulse passes a relay optics to get onto the transmitter telescope and out into the atmosphere.

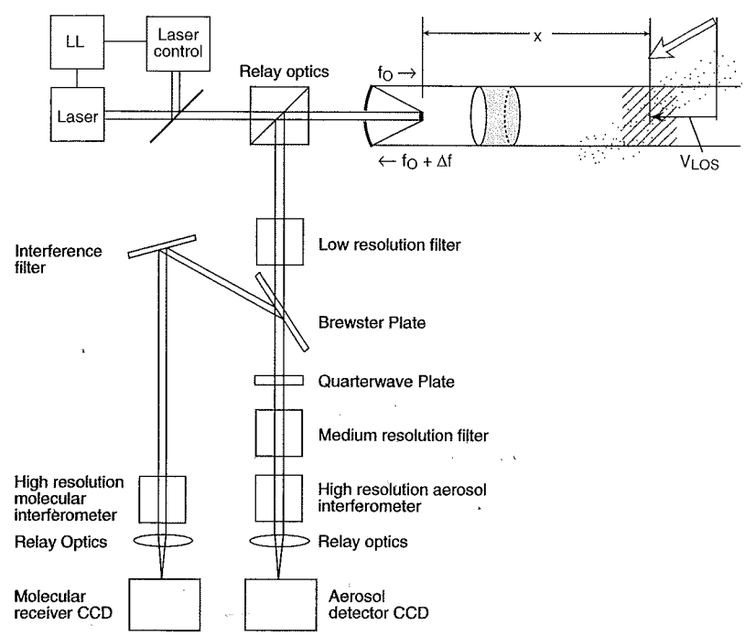

Fig. 12.5. Schematic of a direct-detection lidar.

The backscattered radiation is split into two channels, an aerosol and a molecular channel. Both parts pass several filters and are at the end recorded by a CCD detector. A Fabry–Perot and a Fizeau interferometer are used for the molecular and the aerosol component, respectively. This scheme allows one to partially circumvent the problems associated with the superposition of the broad molecule signal with the narrow aerosol peak. To meet eye-safety requirements, the system works with UV radiation around 0.35 μm.

Heterodyne Detection

In heterodyne detection the return signal is not passed through one or several narrow-band optical filters. Instead, the return signal is mixed with the radiation from a local optical oscillator ("LO"). The mixed signal contains the sum and the difference frequencies of the two components. The sum is way above the frequency cutoff of the detector, but the difference is a low-frequency signal that can be determined with great accuracy. What is needed for heterodyne-detection lidar is thus a pulsed transmitter laser with high frequency stability of the output frequency f_0 and a second, continuous-wave laser with frequency f_{LO}. The mixing results in frequencies $f_{LO} \pm (f_0 + \Delta f)$, where $f_0 + \Delta f$ is the Doppler-shifted frequency backscattered from the atmosphere. Apart from a DC component, the superposition results in a detector current

$$i_{AC} = \rho \left\{ \sqrt{2P_{LO}P(x,\lambda)} \cos[2\pi(f_{LO} - (f_0 + \Delta f))] + \sqrt{2P_{LO}P(x,\lambda)} \cos[2\pi(f_{LO} + (f_0 + \Delta f))] \right\}. \quad (12.7)$$

As mentioned, only the first component, or beat signal

$$i_{DET} = \rho\sqrt{2P_{LO}P(x,\lambda)} \cos[2\pi(f_{LO} - (f_0 + \Delta f))] \quad (12.8)$$

is measured by the detector, with

ρ	the detector sensitivity,
P_{LO}, f_{LO}	the power and frequency of the reference laser, and
$P(x,\lambda)$, $f_0 + \Delta f$	the power and frequency of the backscattered radiation.

The latter two quantities are the only ones that vary with range x.

The frequency difference between the frequency of the transmitted laser pulse, f_0, and the local oscillator, f_{LO}, including the sign of this difference, is determined with great accuracy and maintained as stable as possible during the measurement. It is also a key parameter in the subsequent signal evaluation.

A coherent Doppler lidar (Fig. 12.6) consists in principle of a high-power, frequency-controlled, pulsed laser transmitter (TE), a transmitter-receiver telescope, two heterodyne detectors (D1, D2) in which the local-oscillator radiation is mixed with the outgoing pulse (D1) and with the Doppler-shifted backscatter signal (D2), and a signal processing system (not shown in Fig. 12.6). A locking loop (LL) connects the two lasers. The length of the laser pulse is normally a few microseconds. The temporal distribution of the pulse power is either gaussian (for solid-state lasers) or like a gain-switched spike (for CO_2 lasers). If a CO_2 laser is used at a wavelength around 10.6 μm, a frequency shift Δf of 189 kHz corresponds to a radial velocity component of 1 m/s [21–23].

The optical signal contains speckle which results from constructive and destructive interference of waves scattered by randomly distributed particles. Different shots into the same part of the atmosphere thus lead to different return signals because of the random distribution of the scatterers.

To sum up, heterodyne-detection lidars thus differ from most other lidars by their need for

- a pulsed, narrow-frequency, ultrastable high-power laser,
- a second narrow-frequency laser usually referred to as local oscillator (LO),
- a fast detector in which the return and LO signals are mixed,

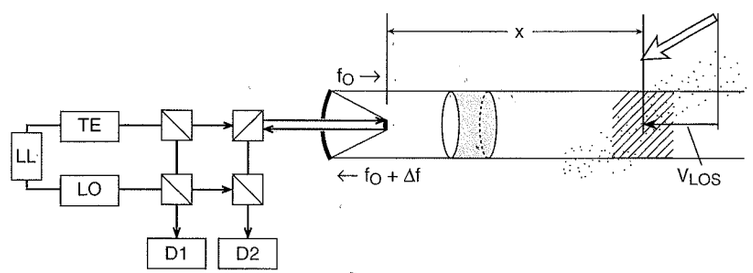

Fig. 12.6. Principle of a heterodyne-detection Doppler lidar.

- a second fast detector in which the transmitted and LO signals are mixed (the so-called pulse monitor),
- the time for averaging over several shots to average out speckle, and
- the presence of aerosol particles.

The main assets of the heterodyne-detection technique are the high tolerance of background light and the independence of temperature and all properties of the optical components of the system.

Figure 12.7 shows an example of a lidar heterodyne signal. One can identify a strong signal near the ground, then a weak signal up to a height of 7.3 km where there are few aerosols present, and then a strong signal from a cirrus cloud that extends up to 9.6 km.

12.4.3 Scan Techniques

As pulsed Doppler lidars measure profiles of the line-of-sight wind velocity, vertically pointed systems directly provide the profile of the vertical wind velocity. For the horizontal wind, the lidars must be tilted out of the vertical. In this way the horizontal wind produces a line-of-sight component to the lidar signal, and with appropriate scanning schemes the three-dimensional wind vector can be inferred [24, 25]. A necessary assumption is horizontal homogeneity of the wind field over the sensed volume. Vertical homogeneity, however, is not required.

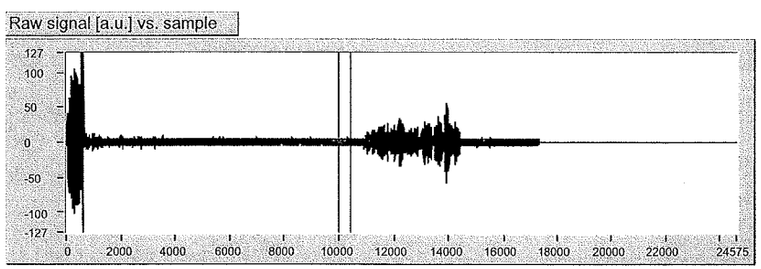

Fig. 12.7. Example of a heterodyne lidar signal. The horizontal axis is time-bin (or "sample") number, i.e., distance, with one sample corresponding to 1.5 m. Because of the paucity of aerosol there is little signal below 7300 m, except for the region close to the ground below about 300 m. The cirrus cloud that begins at 7300 m extends up to 9600 m altitude.

VAD Technique

When a conical scan is carried out with the apex of the cone at the lidar scanner as depicted in Fig. 12.8 and, for a given height or distance, the velocity signal is displayed as a function of azimuth angle, a plot as the one shown in Fig. 12.9 is obtained. From this display of velocity versus azimuth the technique got its name of velocity-azimuth display, or VAD [26, 27]. In the ideal case of a homogeneous atmosphere the measured LOS component shows a sine-like behavior (Fig. 12.9) given by

$$v_r = -u \sin\theta \cos\varphi - v \cos\theta \cos\varphi - w \sin\varphi, \quad \text{with} \tag{12.9}$$

- u the west–east component,
- v the south–north component,
- w the vertical component,
- θ the azimuth angle, clockwise from North, and
- φ the elevation angle.

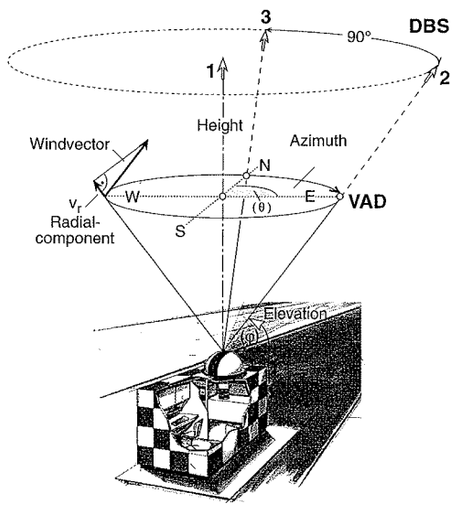

Fig. 12.8. Schematic of the scan technique of a Doppler lidar. Lower part: VAD scan, upper part: DBS scan.

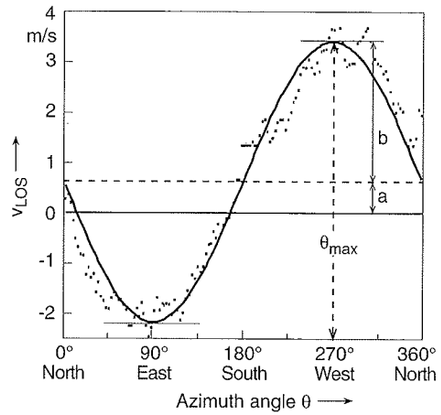

Fig. 12.9. Example of sine fitting of the radial wind velocity simulated with the use of the VAD technique.

If we fit this to a function of type

$$v_r = a + b\cos(\theta - \theta_{max}) \tag{12.10}$$

with offset a, amplitude b, and phase shift θ_{max}, we immediately get the three-dimensional wind vector

$$\mathbf{u} = (u, v, w) = (-b\ \sin\theta_{max}/\cos\varphi, -b\cos\theta_{max}/\cos\varphi, -a/\sin\varphi). \tag{12.11}$$

With this, the horizontal wind speed u_{hor} is

$$u_{hor} = (u^2 + v^2)^{1/2} = b/\cos\varphi, \tag{12.12}$$

the horizontal wind direction dd, as westwind, e.g., blows *from* the west,

$$dd = \theta_{max}, \tag{12.13}$$

vertical wind velocity w, defined as positive for wind *up*, is

$$w = -a/\sin\varphi, \tag{12.14}$$

and total wind speed is

$$|\mathbf{u}| = (u^2 + v^2 + w^2)^{1/2}. \tag{12.15}$$

For a VAD scan, a separate sine-wave fit is done for each height interval. From each of those one set of data a, b, θ_{max} and, consequently, u, v, w is obtained for each height interval.

When used with a ground-based system, these formulas can be used as above. For airborne systems, they must be corrected for the movement of the aircraft. Because the speed of the platform is as a rule much higher than the wind speed, the VAD speed is mainly due to the movement of the airplane, and the contribution from the wind results in a small perturbation. To separate the two, the speed and direction of the aircraft must be known with high accuracy.

The smoothness of the sine-wave fit and thus the precision of its parameters depends on instrumental parameters, but also on turbulence and thus on the roughness of the terrain and on weather data such as atmospheric stratification stability. In addition to such lidar data as pulse-repetition frequency and time-bin width, these other factors must be taken into account if a planned measurement is to yield the desired data in a predetermined time. This applies to the VAD and the DBS scan techniques (see below) in the same manner.

DBS Technique

Under the assumption of cellular flow with little turbulence which would lead to a smooth sinusoidal behavior in the VAD scan, it can be expected that four measurements at azimuth-angle intervals of 90°, or three at 120°, or even two at right angles should be sufficient, along with one measurement in the vertical. For the case of a total of three directions (vertical, tilted east, and tilted north), the three components u, v, w are obtained as follows:

$$u = -(v_{r2} - v_{r1}\sin\varphi)/\cos\varphi, \tag{12.16}$$

$$v = -(v_{r3} - v_{r1}\sin\varphi)/\cos\varphi, \text{ and} \tag{12.17}$$

$$w = -v_{r1}. \tag{12.18}$$

Here v_{r1}, v_{r2}, and v_{r3} are the vertical, east, and north radial velocities, respectively.

This Doppler beam swinging, or DBS, technique is faster and simpler both in the hardware and in the data evaluation algorithm, but lacks the goodness-of-fit information as a measure for the reliability of the results. This shortcoming is partially compensated by information about

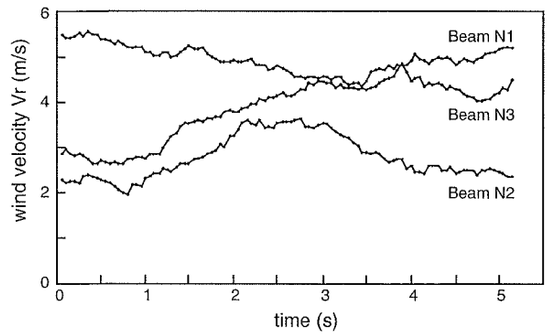

Fig. 12.10. Simulation of the behaviour of turbulent wind components in the boundary layer, from Ref. [27].

the temporal behavior of the data. An example is shown in Fig. 12.10 which presents results of a simulation of high-frequency data obtained from three slant lidar beams oriented such that the projections onto the horizontal plane form three angles of 120°. From data such as those of Fig. 12.10 the degree of smoothing (or temporal integration) necessary to obtain the wind speed and direction data required for a given application can directly be inferred. In addition, turbulence is easily determined for any time scale as dictated by the particular process investigated, particularly as turbulence depends critically on ground roughness length and atmospheric stratification stability.

In principle, the VAD and DBS scan techniques can be combined with both direct-detection and heterodyne-detection Doppler wind lidar systems. As parameters such as maximum range, range resolution, temporal resolution (or scan rate), and wind-speed and wind-direction sensitivity all depend on one another and in a somewhat different way for VAD and DBS scans, these dependencies must be known and observed when planning a measurement for a given purpose.

12.5 Systems and Applications

There are numerous wind lidar systems in operation and even more in the planning and construction phase today. Only a small fraction of them can be mentioned here. The selection has not been made according to "seniority" or ancientness; instead, we have been trying to show what diverse applications can profit from Doppler wind lidar.

Historically, heterodyne-detection Doppler lidars were the first to offer accurate, dependable results on a routine basis. Direct-detection systems, simpler in design although more critical in components, adjustment and stability, are in a way lagging behind. Following the order in which the two detection schemes have been treated in this chapter, we first briefly describe a direct-detection system built in France and then present different applications of heterodyne-detection lidars, until now the workhorse of Doppler wind lidar. The section concludes with the presentation of a continuous-wave (cw) lidar and another system previously considered as being classified as on the borderline between long-range, depth-resolving lidars and shorter-range non-lidar systems, a laser Doppler velocimeter.

12.5.1 Direct-Detection Lidar of the OHP

The Doppler wind lidar of the Observatoire de Haute Provence (OHP) at Saint-Jean-l'Observatoire, France, uses a frequency-doubled, well frequency-stabilized Nd:YAG laser which emits in the green. Laser pulses are sequentially transmitted to three separate telescopes, one oriented vertical, the other two north and east at elevation angles of 55°. The aerosol and molecular scattering components of the return signals are separated using the double-edge technique with a Fabry–Perot interferometer (FPI). Its characteristics have been determined experimentally and least-squares-fitted to the transmission function of a spatially homogeneous FPI. However, the measured calibration curve turned out to be more complex, and the actual transmission function takes into account residual surface inhomogeneities [28, 29]. Figure 12.11 shows the system layout of the OHP direct detection Doppler lidar.

Calibration of the system is carried out when the lidar beam is pointed to the zenith, under conditions of zero wind [29]. When taking measurements, the vertical wind is used as a correction in the evaluation procedure of the horizontal components. Measurement time is typically one minute for each of the three directions. For daylight operation a special procedure is applied to remove the skylight background.

12.5.2 Boundary-Layer Flow Measurements with the NOAA Heterodyne Doppler Wind Lidar

Among the many Doppler wind lidars built at the National Oceanic and Atmospheric Administration (NOAA) laboratory at Boulder, CO, one

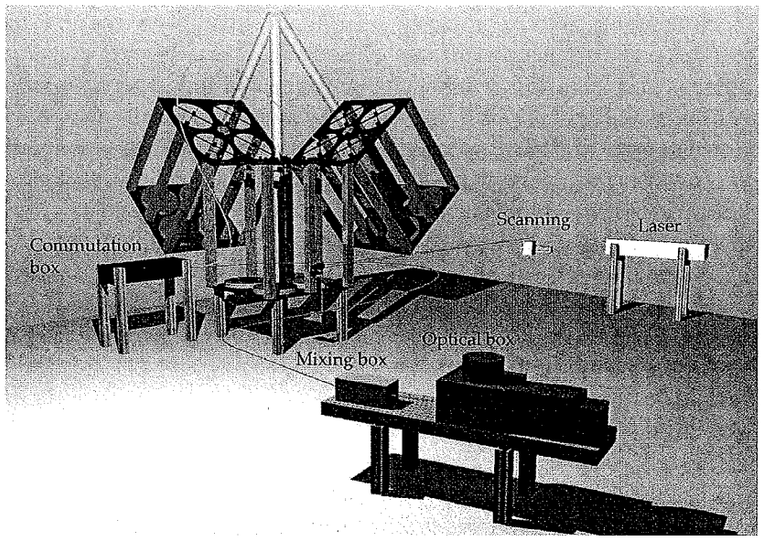

Fig. 12.11. OHP direct-detection Doppler lidar design.

of the more recent instruments is the Mini-MOPA system. It is a design based on a CO_2-laser Doppler system using a seed laser, or master oscillator (MO), injecting narrow-bandwidth radiation into a second laser, the power amplifier (PA). The system has selectable wavelengths between 9 and 11 μm, 2 mJ output energy, and 300 Hz pulse repetition rate. The maximum range limited by the digitizer is 18 km, with a range resolution that can be selected between 45 and 300 m. The system has been used in many campaigns and is semiautomated, allowing hands-off operation for several hours.

One of the impressive applications of such a Doppler lidar is the representation of the flow in the boundary layer [30]. Figure 12.12 gives an example. This image of the color-coded LOS wind component on an area covering a half-circle of about 8 km radius explains different flow situations from the mountains and back together with the normal wind from the southern basin.

12.5.3 Airborne Heterodyne Lidar Within the WIND Project

A relatively recent heterodyne Doppler wind lidar system is the one developed under the Wind INfrared Doppler (WIND) lidar project. It

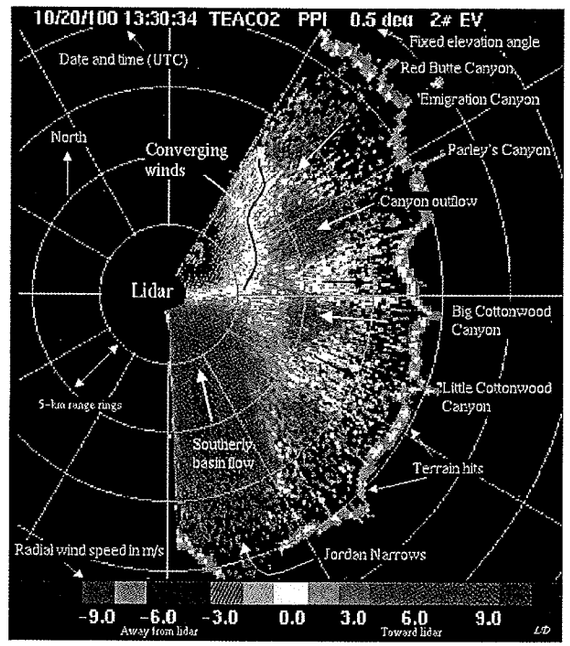

Fig. 12.12. Near-horizontal (0.5°-elevation) azimuthal scan of radial wind velocity [30].

is an airborne system based on the familiar CO_2 laser concept. The project [31], a French–German cooperation of the Centre National de la Recherche Scientifique (CNRS) and the Centre Nationale d'Etudes Spatiales (CNES) with the Deutsches Zentrum für Luft- und Raumfahrt (DLR), is characterized by two objectives. The first is a significant contribution to mesoscale meteorology by investigation of phenomena like the influence of orography on atmospheric flows, land–sea interaction, the dynamics of convective and stratiform clouds, and the transport of humidity. This defines the requirements on spatial resolution of 250 m in height with a grid size of $10 \times 10\,\mathrm{km}^2$ and on velocity accuracy of 1 m/s for the horizontal wind component. The second objective is to act as a precursor for the spaceborne global wind measurement system AEOLUS, the Atmospheric Explorer for Observations with Lidar in the Ultraviolet from Space, in the framework of the ESA Atmospheric Dynamics Mission (ADM); such a system is scheduled for launch in 2007 (cf. Chapter 13 of this

book). Airborne Doppler lidars were used in the past [32–35] and are applied also as precursor experiments for spaceborne application of the technique [35].

A validation flight was carried out on 12 October 1999, 13:30 UTC. The wind profiler radar (WPR) [36] of the Meteorological Observatory Lindenberg (MOL) of the German Weather Service DWD was used as the reference instrument, extrapolation to more remote areas was done with the local model (LM) of the DWD. This model has a horizontal resolution of 7 km. It is a non-hydrostatic model with 35 altitude levels and includes turbulent vertical exchange. Airborne wind lidar systems are expected to meet at least the accuracy and horizontal-resolution specifications of state-of-the-art numerical models [37].

Figure 12.13 shows the result of the wind profile determination. Within the statistical variations, the agreement is perfect.

The WIND instrument is a flexible and modular system for airborne measurements of mesoscale wind phenomena. It provides actually an accuracy of 1 m/s for the horizontal wind in a volume of the size of

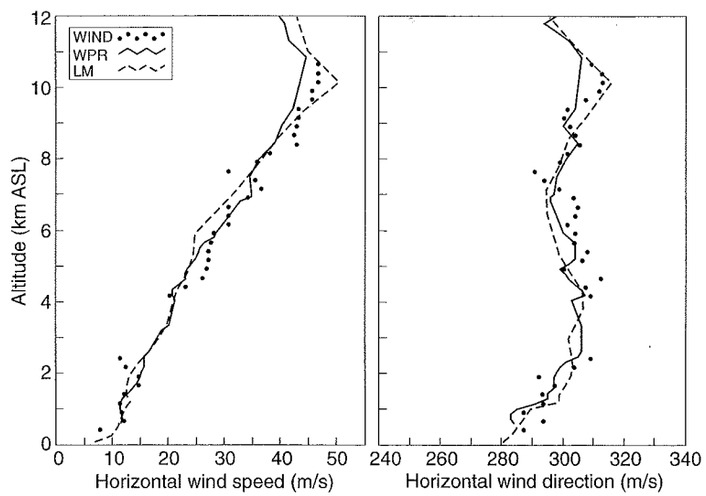

Fig. 12.13. Comparison of wind profiles determined with the WIND instrument (dotted lines), the radar wind profiler (WPR, solid lines), and the WPR data extrapolated to the area covered by the WIND system (dashed line). WIND data comprise 5 conical scans, or >100 s of measurement time, in a $10 \times 50\,\mathrm{km}^2$-size horizontal grid. WPR data are averaged over 30 minutes. Note the suppression of zero in the wind-direction scale.

10 km × 50 km × 250 m in the boundary layer. An improvement of the resolution to 10 km × 10 km × 250 m appears realistic as a near-future goal. Other uses in the scanning or non-scanning mode are also possible, e.g., the determination of single line-of-sight wind profiles to simulate the performance of spaceborne Doppler lidars.

12.5.4 Ground-Based Continuous-Wave Heterodyne Lidar for the Measurement of Wake Vortices

The measurement principle for determining aircraft wake vortices with a Doppler wind lidar is illustrated in Fig. 12.14. These inhomogeneities of the wind-field vector can be dangerous to aircraft, especially in landing operations. Every plane, when in flight, generates in its wake a pair of counterrotating horizontal vortices. When planes fly behind one another in close succession, wake vortices can present a considerable hazard. At present the U.S. Federal Aviation Administration (FAA) mandates minimum distances for aircraft during instrument landing conditions. These differ with airplane size. There are three categories: heavy, large, and small.

These wake vortices are invisible to the eye, but can be detected with Doppler wind lidar. The lidar scans the air volume in a vertical plane perpendicular to the landing runway. The radial velocity can reach values around 20 m/s, depending on the type of aircraft, its weight and its takeoff velocity. It can be used to calculate the rotational velocity of the vortex. The scheme of the measurement is sketched in Fig. 12.14. The change in v_{LOS} caused by the vortex, divided by the cosine of the

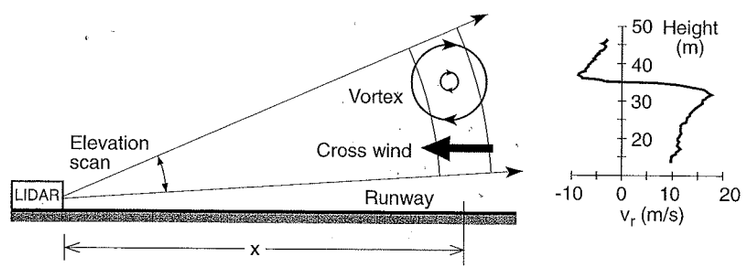

Fig. 12.14. Left, measurement principle for determining aircraft wake vortices with a Doppler wind lidar. v_{r} radial or line-of-sight wind velocity. Right, vertical distribution of crosswind at distance x (which might be the position of the landing-runway centerline).

lidar elevation angle, directly yields the amount and spatial distribution of excess cross wind for the landing airplane [38, 39].

Continuous-wave CO_2-laser Doppler lidars like the one used here are in operation at the French Office National d'Études et de Recherches Aérospatiales (ONERA), the Deutsches Zentrum für Luft und Raumfahrt (DLR), and the Massachusetts Institute of Technology (MIT) in the United States. The European Community has started a program to both detect and forecast wake vortices. For a better range resolution pulsed systems (2-μm laser Doppler system from Coherent Technologies (CTI, http://www.ctilidar.com)) are used [40]. The parameters of such a lidar are listed in Table 12.1.

Clearly, large-aircraft wake vortices are not stationary. Their displacement can easily be followed with lidars. Figure 12.15 shows an example of the determined position of the core of the vortex.

12.5.5 Clear-Air Turbulence

A key application of Doppler wind lidar to aircraft safety is also the measurement of clear-air turbulence (CAT), a hazard hard to determine with any other means. Considerable progress has been made in this important field in recent years. Figure 12.16 shows a time-series plot of the velocity estimates, along with *in situ* true-airspeed (TAS) measurements. As can

Table 12.1. Main parameters of the 2-μm pulsed Doppler lidar

Slave laser:	Type	Tm:LuAG
	Wavelength	2022.54 nm
	Pulse energy	2.0 mJ
	Pulse length (FWHM)	400 ± 40 ns
	Pulse repetition rate	500 Hz
	LO/SO frequency offset	102 ± 3 MHz
Telescope:	Type	off-axis
	Aperture	108 mm
Scanner:	Oscillating mirror vertical scan range	≥20°
	Scan duration	≈11 s
	Fly-back time	≈0.5 s
Data acquisition:	Concept of early digitizing	
	Sampling rate	500 MHz
	Sample length	0.3 m
Measurement range:	Processed data	500–1100 m
Spatial resolution:	Along LOS	3 m
	Perpendicular to LOS	0.9–1.9 m

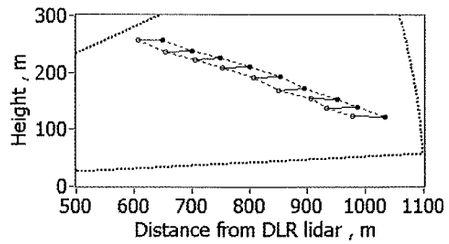

Fig. 12.15. Wake vortices of large aircraft measured on 13 June 2002 with the DLR wake vortex lidar. Trajectories of port vortex (open circles) and starboard vortex (full circles) observed during 9 consecutive scans.

be seen, due to CAT the radial velocities at different ranges in front of the aircraft vary by >20 m/s or >70 km/h within 3 minutes.

12.5.6 Remote Wind Speed Measurements for Wind Power Stations

Installations that also critically depend on wind speed and direction are wind power stations. If blade pitch and rotor orientation are properly adapted to the prevailing wind, then both efficiency and safety of the facility can be maximized. However, the feedback mechanism of the

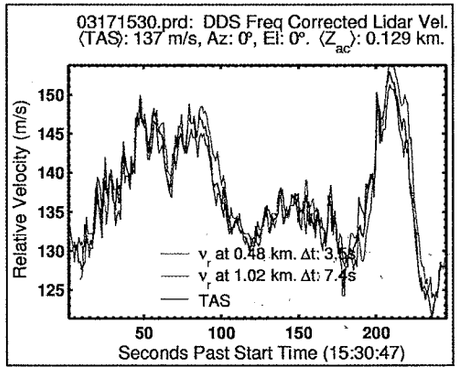

Fig. 12.16. Velocity versus time for an airborne clear-air turbulence Doppler lidar [40]. The three traces represent the lidar measurement 3.5 s or 0.48 km (blue) and 7.4 s or 1.02 km (green) ahead of the time of passage, as a function of distance, and the result of the *in situ* (true airspeed, TAS) measurement (red trace).

systems is too slow to adequately follow changes in wind speed and direction. It is therefore necessary to measure these quantities at a distance of roughly 150 m windward of the turbine.

It may seem as if a lidar was needed for the purpose. However, this is not the case. A normal cw laser Doppler velocimeter (cf. Section 3.3) will be perfectly sufficient for the purpose. A corresponding system for installation at the top of the turbine is currently under development [41]. First tests with a CO_2-laser source have shown encouraging results.

12.6 Future Developments

Like most other lidar developments, wind lidar is also a field in which instruments are continuously improved, reduced in size, weight, power consumption, and cost. Instruments are getting more highly integrated to make them easier to align, adjust and operate. Simultaneously and partially caused by this instrument improvement process, the number of fields in which wind lidar systems are being used increases. The development [42] as well as the new uses are greatly facilitated if a certain standardization takes place. In this section one example is given for each of these tendencies to show in which direction near-future work in wind lidar is likely to go.

12.6.1 Instruments

In the field of instruments, work toward spaceborne systems is of course one of the important items (cf. Chapter 13 of this book). This development started as soon as the end of the 1980s [43, 44] and is in full swing today. What is new, however, is an "instrument" that is sheer software and which we call a virtual instrument. Virtual instruments [45] represent powerful tools to test and investigate system performance in various combinations of components and under varying atmospheric conditions without any hardware development. The data sets generated with such virtual instruments can be used to submit components to further tests, to try out new ones, to improve and validate program modules like signal processors, and to carry out virtual experiments.

In the DLR virtual Doppler lidar (see Fig. 12.17) the parameters that can be varied include laser wavelength, pulse power, and transceiver characteristics. The pulse shape can be either gaussian (as for solid-state lasers) or spiked (as for CO_2 lasers). Detection can be direct or of the

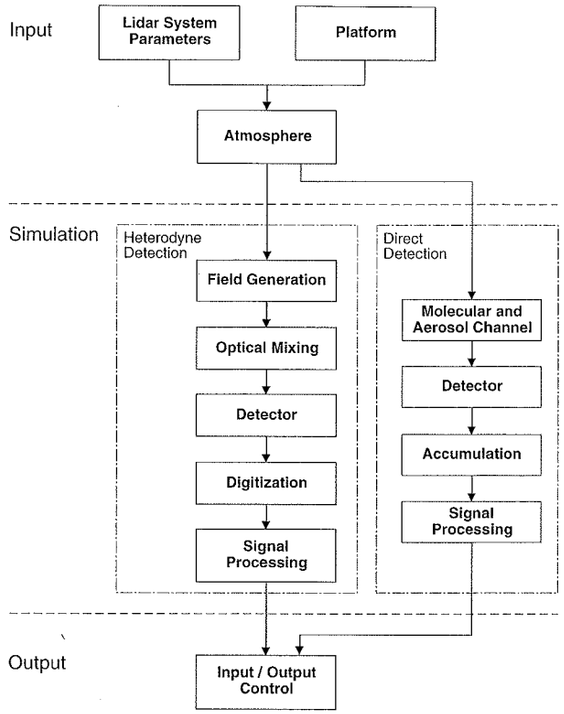

Fig. 12.17. Block diagram of the DLR virtual instrument.

heterodyne type. The platform can be chosen to be an aircraft, satellite, or ground-based station, all with characteristic parameters. For the virtual lidar the atmosphere is "sliced" into height intervals of 1.5 m minimum thickness. In the slices the optical beam is scattered and absorbed with uniform coefficients β and α. Clouds strongly affect the values of both β and α. Noise is generated with a module called AGNA, for Additive Gaussian Noise Approximation; AGNA was originally developed at the Technical University (TU) Vienna [46]. In the digitization and signal-processing modules a number of options is available including a variant in which return signals are treated pair by pair (pulse-pair or PP mode), and one that observes the criterion of maximum likelihood (ML mode). The direct-detection virtual instrument can work on two techniques, the double-edge (for the exploitation of the molecular signal) and the multichannel-Fizeau technique (for the aerosol signal). The system

is written in LabVIEW©. Its result is the comparison of a calculated ("measured") wind profile with the input, or "true," profile.

There are other virtual instruments as well. One of them is based upon the Delphi Study of ESA [46] and the improved ALIENS simulator [47]. By adding scanning capability and the possibility to operate aboard a moving platform, a new dynamic version of a virtual instrument is obtained. For "experiments" it requires a three-dimensional model of the atmosphere.

12.6.2 Weather Forecast

A field that heavily relies on the availability of high-accuracy, high-resolution wind data is meteorology. The lack of global wind data is indeed one of the major deficiencies of the current meteorological network. In fact, one of the hot candidates to provide a great deal of the necessary wind parameters is a future spaceborne Doppler lidar [48, 49]. To determine exactly what is needed and which configuration will provide the most reliable results can no better be determined than with one of the virtual lidar instruments described above. A study is actually under way to estimate the effect of lidar winds on numeric weather prediction [50].

12.6.3 Standardization

Work that is done independently in different places necessarily creates different technical terms for the same objects and notions. Different parameter values are chosen as the basis for key performance characteristics. Different procedures are followed when a measurement or measurement campaign is planned, prepared and carried out and when the data are processed, evaluated and presented. Often certain of those procedures proved technically superior to others. To make the corresponding knowledge publicly available, guidelines proved very useful. Not only do these recommendations help the manufacturers, they also allow users to decide whether or not the lidar technique can meet their goal, to clarify their expectations and to specify their requirements on a lidar for a given purpose. The Doppler wind guideline of the German Commission on Air Pollution Prevention [42] was one of the first to appear in a series of guidelines on quantitative remote sensing techniques and served as a kind of model to the other ones that followed [51].

References

[1] R. Heilmann, J. Kuschel: Electronics Letters **29**, 810 (1993)
[2] J.T. Sroga, E.W. Eloranta, T. Barber: J. Appl. Met. **19**, 598 (1980)
[3] Y. Sasano, H. Hirohara, T. Yamazaki, et al.: J. Appl. Met. **21**, 1516 (1982)
[4] L. Lading, A.S. Jensen, C. Fog, et al.: Appl. Opt. **17**, 1486 (1978)
[5] K.G. Bartlett, C.Y. She: Opt. Lett. **1**, 175 (1977)
[6] C.Y. She, R.F. Kelley: J. Opt. Soc. Am. **72**, 365 (1982)
[7] E. Durst, E. Ernst, J. Volklein: Z. f. Flugwissenschaften und Weltraumforschung **11**, 61 (1987)
[8] B. Ruck: *Laser-Doppler-Anemometrie* (AT Fachverlag, Stuttgart 1987)
[9] A. Brown, E.L. Thomas, R. Foord, et al.: J. Phys D **11**, 137 (1978)
[10] R.L. Schwiesow, R.E. Cupp: Appl. Opt. **20**, 579 (1981)
[11] A.A. Woodfield, J.M. Vaughan: Int. J. Aviation Safety **1**, 129 (1983)
[12] R.J. Keeler, R.J. Serafin, R.L. Schwiesow, et al.: J. Atm. Ocean. Tech. **4**, 113 (1987)
[13] L. Kristensen, D.H. Lenschow: J. Atm. Ocean. Tech. **4**, 128 (1987)
[14] G. Tenti, C.D. Boley, R.C. Desai: Canadian Journ. of Physics **52**, 285 (1974)
[15] C.L. Korb, B.M. Gentry, S.X. Li, et al.: Appl. Opt. **37**, 3097 (1998)
[16] M.J. McGill, W.D. Hart, J.A. McKay, et al.: Appl. Optics **38**, 6388 (1999)
[17] M.-.L. Chanin, A. Garnier, A. Hauchecorne, et al.: Geophys. Res. Letters **16**, 1273 (1989)
[18] D. Rees, G.K. Nelke, K.H. Fricke, et al.: J. Atmos. Terr. Phys. **58**, 1827 (1996)
[19] M. Schillinger, D. Morancais, F. Fabre, et al.: Proc. SPIE **5234**, 40 (2003)
[20] A. Garnier, M.-L. Chanin: Appl. Phys. B **55**, 35 (1992)
[21] M.J. Post, R.E. Cupp: Appl. Opt. **29**, 4145 (1990)
[22] J.M. Vaughan, D.W. Brown, J. Rothermel, et al.: Proc. OSA Coherent Laser Radar Meeting, Aspen, CO (1987)
[23] J.W. Bilbro, C. DiMarzio, D. Fitzjarrald, et al.: Appl. Opt. **25**, 3952 (1986)
[24] F. Köpp, H. Herrmann, C. Werner, R. Schwiesow: DFVLR-FB 83-11 (1983)
[25] R. Schwiesow, F. Köpp, C. Werner: J. Atmosph. Oceanic Technology **2**, 3 (1985)
[26] R.M. Lhermitte, D. Atlas: Proc. 9th Weather Radar Conference, Boston, Americ. Meteor. Soc. **218**, (1966)
[27] V.A. Banakh, I.N. Smalikho, F. Köpp, et al.: Appl. Optics **34**, 2055 (1995)
[28] C. Souprayen, A. Garnier, A. Herzog, et al.: Appl. Optics **38**, 2410 (1999)
[29] C. Souprayen, A. Garnier, A. Herzog: Appl. Optics **38**, 2422 (1999)
[30] R.M. Banta, L.S. Darby, J.D. Fast, et al.: J. Appl. Meteor. **43**, 1348 (2004)
[31] C. Werner, P. Flamant, O. Reitebuch, et al.: Opt. Eng. **40**, 115 (2001)
[32] J.W. Bilbro, W.W. Vaughan: Bull. Am. Meteorol. Soc. **59**, 1095 (1978)
[33] J.W. Bilbro, J.G. Fichtl, D. Fitzjarrald, et al.: Bull. Am. Meteor. Soc. **65**, 348 (1984)
[34] E.W. McCaul, R.J. Doviak: Accuracy of aircraft position and motion data from inertial navigation equipment aboard the NASA CV 990. NASA final report, Contract No. H-84050B (1988)
[35] J. Rothermel, D.R. Cutten, R.M. Hardesty, et al.: Bull. Amer. Meteor. Soc. **79**, 581 (1998)
[36] H. Steinhagen, J. Dibbern, D. Engelbart, et al.: Meteorolog. Zeitschrift N.F. **7**, 248 (1998)

[37] O. Reitebuch, C. Werner, I. Leike, et al.: JTECH **18**, 1331 (2001)
[38] F. Köpp: AIAA J. **32**, 2055 (1994)
[39] F. Köpp, S. Rahm, I. Smalikho: J. Atmos. Oceanic Technology **21**, 194 (2004)
[40] S.M. Hannon, P. Gatt, S.W. Henderson, et al.: Proceedings 12th Coherent Laser Radar Conference, Bar Harbor, ME, 15–20 June 2003, 86 (2003)
[41] R.S. Hansen, G. Miller: Proceedings 11th Coherent Laser Radar Conference, Malvern, U.K., 1–6 July 2003, 123 (2001)
[42] KRdL German Commission on Air Pollution Prevention (VDI): *VDI 3786 Part 14: Environmental meteorology—Ground-based remote sensing of the wind vector–Doppler wind LIDAR* (Beuth Verlag, Berlin 2001)
[43] LAWS: Laser Atmospheric Wind Sounder: NASA Instrument Panel Report Vol IIg, Earth Observing System (1987)
[44] ALADIN, Atmospheric Laser Doppler Instrument–ESA SP-1112 (1989)
[45] I. Leike, J. Streicher, V. Banakh, et al.: JTECH **18**, 1447 (2001)
[46] P. Winzer, W. Leeb, I. Leike, et al.: Coherent Detection at Low Photon Number per Measurement Interval (DELPHI). ESA/ESTEC Contract No. 11733/95/NL/CN (1997)
[47] J. Streicher, I. Leike, C. Werner: Proc. SPIE **3583**, 380 (1998)
[48] A. Stoffelen, B. Becker, J. Eyre, et al.: Theoretical Studies of the Impact of Doppler Wind Data—Preparation of a Data Base. ESA-CR(P)-3943 (1994)
[49] A. Hollingsworth, P. Lönnberg: The verification of objective analysis: Diagnostics of analysis system performance. ECMWF Technical Report No. 142 (1987)
[50] A. Cress, W. Wergen: Meteorologische Zeitschrift **10**, 91 (2001)
[51] C. Weitkamp, L. Woppowa, C. Werner, et al: In *Lidar Remote Sensing in Atmosphere and Earth Sciences. Reviewed and revised papers presented at the twenty-first International Laser Rader Conference (ILRC21), Québec, Canada, 8–12 July 2002*. L.R. Bissonnette, G. Roy, G. Vallée, eds. (Defence R&D Canada Valcartier, Val-Bélair, QC, Canada), Part 1, p. 15